

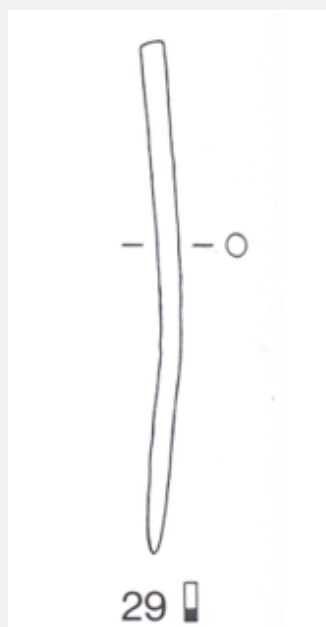
# PIN WITHOUT HEAD HR-18152 – TIN BRONZE – LATE BRONZE AGE – SWITZERLAND

**Artefact name** Pin without head HR-18152

**Authors** Marianne. Senn (Empa, Dübendorf, Zurich, Switzerland) & Christian. Degrigny (HE-Arc CR, Neuchâtel, Neuchâtel, Switzerland)

**Url** /artefacts/912/

## ✧ The object



Credit HE-Arc CR.

Fig. 1: Pin without head (after Rychner-Faraggi 1993, plate 74.29),



Credit HEI Arc, S.Ramseyer

Fig. 2: Dense and smooth brown-yellow patina (detail) of the pin with lacuna showing the underlying metal with location of Fig. 4 (red rectangle),

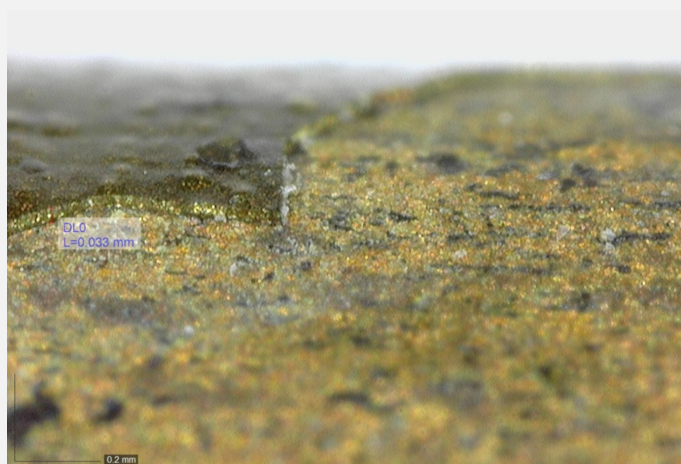
## Description and visual observation

Description of the artefact	Pin without head and smooth brown-yellow patina typical of lake context (Figs. 1-2). Dimensions: L = 7,5cm; Ø = 3.3mm; WT = 4g.
Type of artefact	Pin
Origin	Hauterive - Champréveyres, Neuchâtel, Neuchâtel, Switzerland
Recovering date	Excavation 1983-1985, object from layer 3 to 5
Chronology category	Late Bronze Age
chronology tpq	1054 B.C. ▼
chronology taq	1000 B.C. ▼
Chronology comment	Hallstatt B1 (1054/1037BC _ 1000BC)
Burial conditions / environment	Lake
Artefact location	Laténium, Neuchâtel, Neuchâtel
Owner	Laténium, Neuchâtel, Neuchâtel
Inv. number	Hr 18152
Recorded conservation data	N/A

## Complementary information

Smooth and dense brown-yellow patina has been extensively described by Schweizer (Schweizer 1994).

## Study area(s)



Credit HEI Arc, C,Cevey.

Fig. 3: Side view of a lacuna with the stratigraphy of the brown-yellow patina.

Fig. 4: SEM image of the pin from Fig. 2 (detail), BSE -mode. The crack between the remaining metal and the corrosion layers is clearly visible and the smooth layer below is CP3,

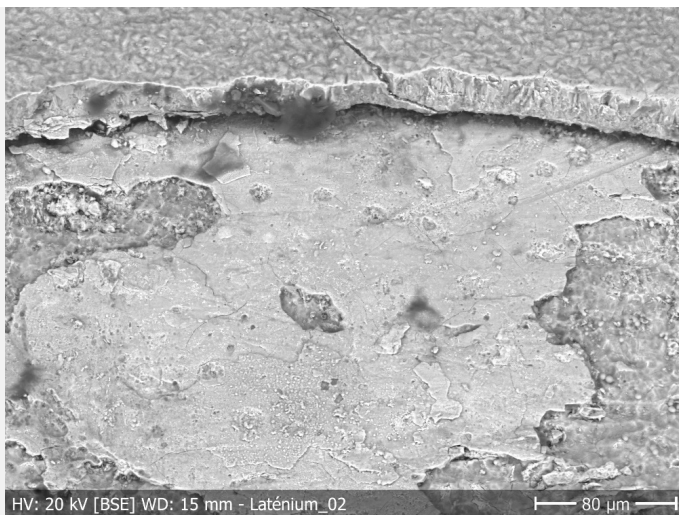


Fig. 5: Location of sampling area,

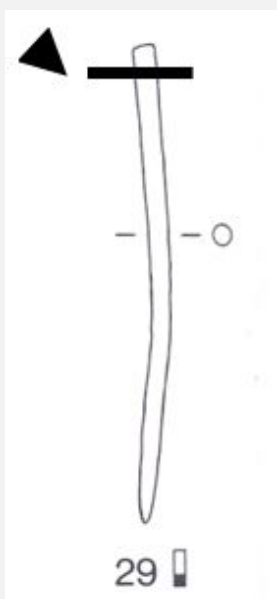
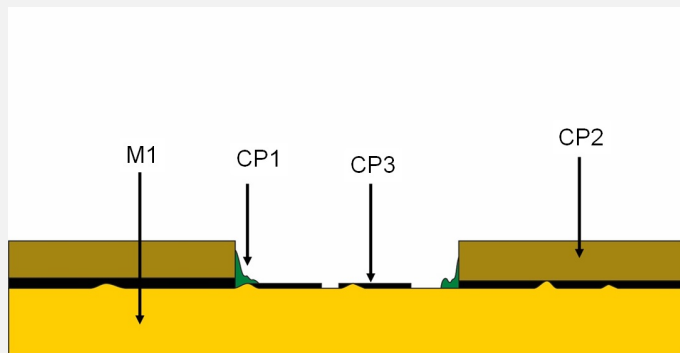


Fig. 6: Cross-section of the pin and remaining material,



#### ✧ Binocular observation and representation of the corrosion structure

The schematic representation below gives an overview of the corrosion layers encountered on the pin from a first visual macroscopic observation.



Credit HEI Arc, N, Gutknecht.

Fig. 7: Stratigraphic representation of the pin without head by macroscopic observation (under binocular),

#### ✖ MiCorr stratigraphy(ies) – Bi

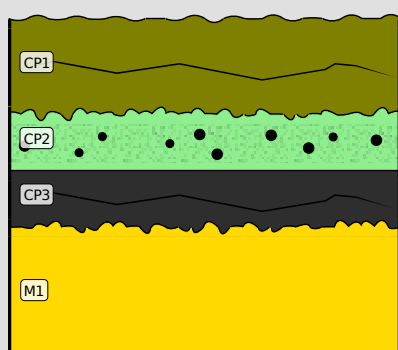
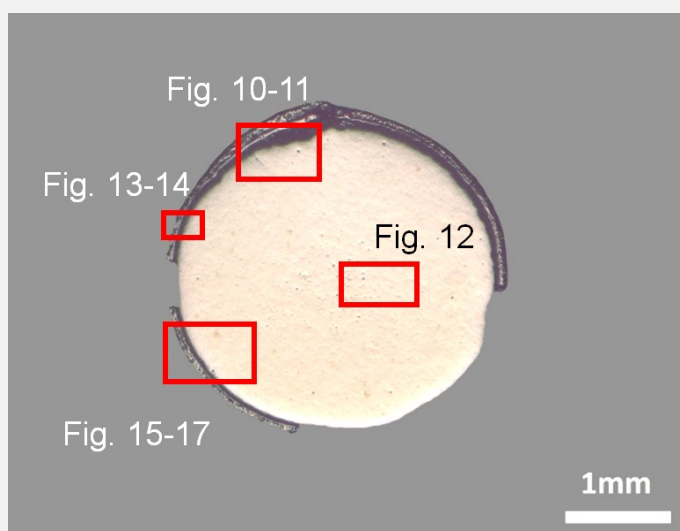


Fig. 8: Stratigraphic representation of the pin without head under binocular using the MiCorr application. The characteristics of the strata are only accessible by clicking on the drawing that redirects you to the search tool by stratigraphy representation, Credit HE-Arc CR.

#### ✖ Sample(s)



Credit HE-Arc CR.

Fig. 9: Micrograph of the cross-section of the sample taken from the pin without head showing the location of Figs. 10 to 17,

#### Description of sample

The cross-section is circular and is a complete section through the pin (Figs. 5 and 6). It is covered with a rather thin and regular (in thickness) corrosion crust (Figs. 3 and 4). One third of the corrosion crust is missing (Fig. 9).

#### Alloy

Tin Bronze

Technology	Annealed after cold working
Lab number of sample	MAH 87-194
Sample location	Musées d'art et d'histoire, Genève, Geneva
Responsible institution	Musées d'art et d'histoire, Genève, Geneva
Date and aim of sampling	1987, metallography and corrosion characterisation

#### Complementary information

This sample is mentioned in Schweizer, 1994.

#### ✧ Analyses and results

##### *Analyses performed:*

Metallography (etched with ferric chloride reagent), Vickers hardness testing, XRF, ICP-OES, SEM/EDS, XRD, Raman spectroscopy.

#### ✧ Non invasive analysis

None.

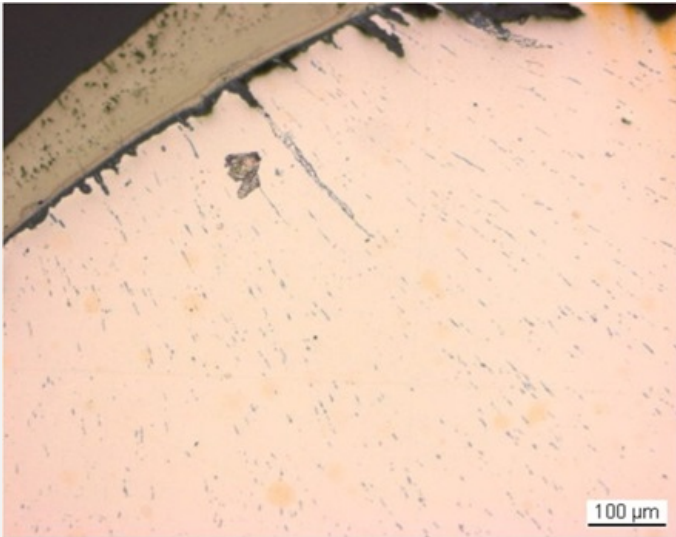
#### ✧ Metal

The remaining metal is a tin bronze and contains copper sulphide as well as heavy metal (Pb-rich) inclusions (Table 1, Figs. 10 and 11). Close to the surface of the remaining metal, copper sulphide inclusions are elongated and form rows (Fig. 10). The etched structure of the tin bronze shows polygonal grains; some of them are twinned (Fig. 12). In the centre of the sample and on the edges, the grains are smaller. The copper sulphide inclusions are located at the grain boundaries and in the grains. The average hardness of the metal is about HV1 110.

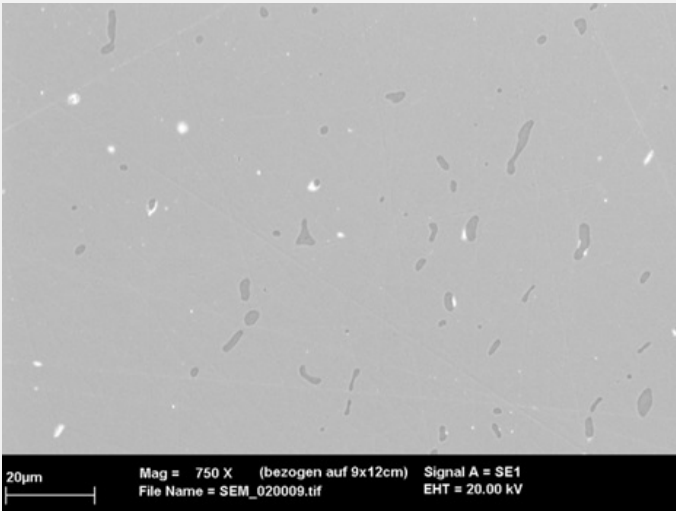
Elements	Cu	Sn	Pb	Sb	As	Ag	Fe	Ni	Co	Zn
mass%	89.22	9.57	0.34	0.26	0.19	0.15	0.09	0.05	0.06	0.05

Table 1: Chemical composition of the metal. Method of analysis: ICP-OES, Laboratory of Analytical Chemistry, Empa.

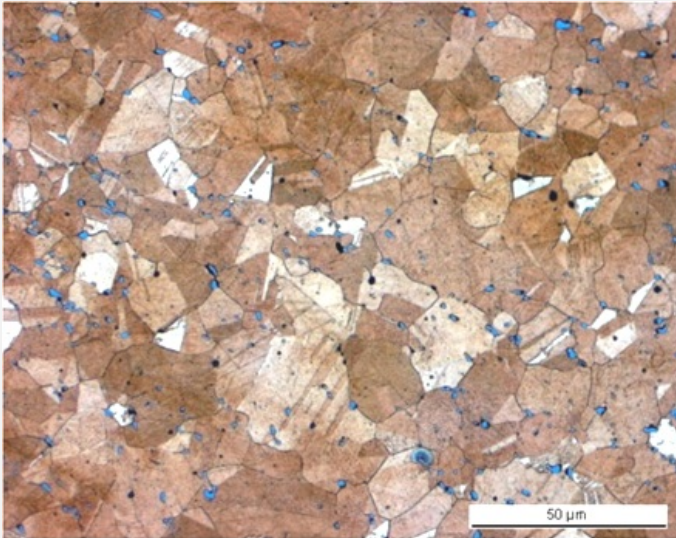
Fig. 10: Micrograph of the metal sample from Fig. 9 (detail), unetched, bright field. Rows of elongated copper sulphide inclusions can be observed,



Credit HE-Arc CR..



Credit HE-Arc CR.



Credit HE-Arc CR.

Fig. 11: SEM image of the metal sample from Fig. 9 (detail), SE-mode. Elongated copper sulphide inclusions (dark-grey) are visible as well as heavy metal (Pb-rich) inclusions (white),

Fig. 12: Micrograph of the metal sample from Fig. 9 (detail), etched, bright field. The metal shows a structure of polygonal and twinned grains. Copper sulphide inclusions are visible as blue spots,

Microstructure	Polygonal and twinned grains
First metal element	Cu
Other metal elements	As, Ag, Sn, Sb, Pb



### Complementary information

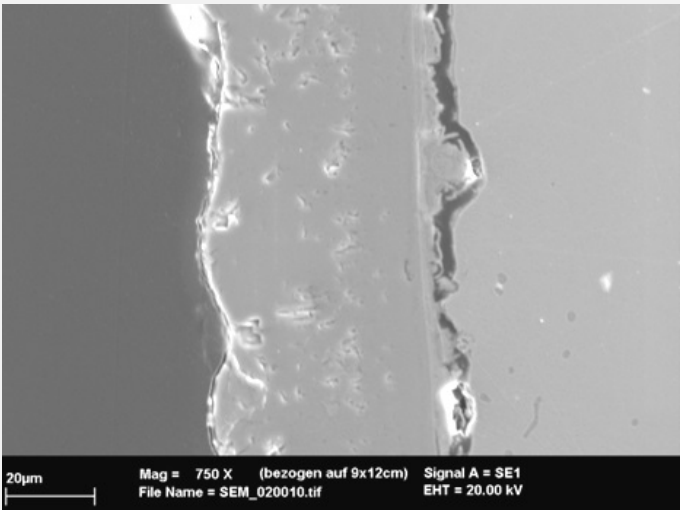
Schweizer (1994) indicates that the copper-tin alloys similar to the one of the pin have minor constituents that were certainly not added intentionally. Furthermore, he mentions that there is no systematic composition difference between bronzes with a lake patina and those with a land patina.

### Corrosion layers

The corrosion crust (patina) is regular in thickness (around 50µm, Fig. 4). It presents lacuna (Fig. 2) and in some areas it is missing completely (Fig. 9). At the metal – corrosion crust interface, there is a crack showing that the latter has separated from the metal core along its whole length (Figs. 4, 9, 10, 13-14). The corrosion crust can be divided into three distinct layers (CP1-3). Directly above the crack is a first dense but cracked and irregular inner layer (CP3, Figs. 4, 13-14). In bright field it appears brown (Fig. 15), in normal and polarised light dark brown (Figs. 2 and 16). It is separated from the adjacent layer by a clear line (Figs. 14 and 15). The second layer (CP2) is dense with little porosity (Figs. 13 and 14). In bright field it appears light brown (fig. 15), in polarised dark dark yellow (Fig. 16). The third and outermost layer (CP1) appears light brown under normal light (Fig. 3) and in bright field (Fig. 15), contains particles (Fig. 14) and is very porous (visible as golden reflections under polarized light, Fig. 16). These results are entirely consistent with Schweizer's observations (Schweizer 1994). The elemental chemical distribution of the SEM image selected reveals that the inner layer (CP3) is depleted in Cu, but rich in Sn, O and Si (Fig. 17 and Table 2) and its interface with the intermediate layer (CP2) could represent the limit of the original surface (Figs. 14 and 17). The second and third layer (CP2 and CP1) are Fe, Cu and S-rich (Fig. 17) and have a composition similar to chalcopyrite/CuFeS<sub>2</sub> (Table 2). This was confirmed by XRD. The particles (inclusions) have a composition similar to covellite or covellite/CuS (Table 2). Both chalcopyrite and covellite have been identified by Raman spectroscopy (Figs. 18 and 19).

Elements	S	Fe	Cu	O	Si	Sn	Total
CP1 and CP2	35	30	34	<	<	<	99
Particles in CP1	26	4.1	68	<	<	<	98
CP3	5.8	5.0	13	32	2	41	99

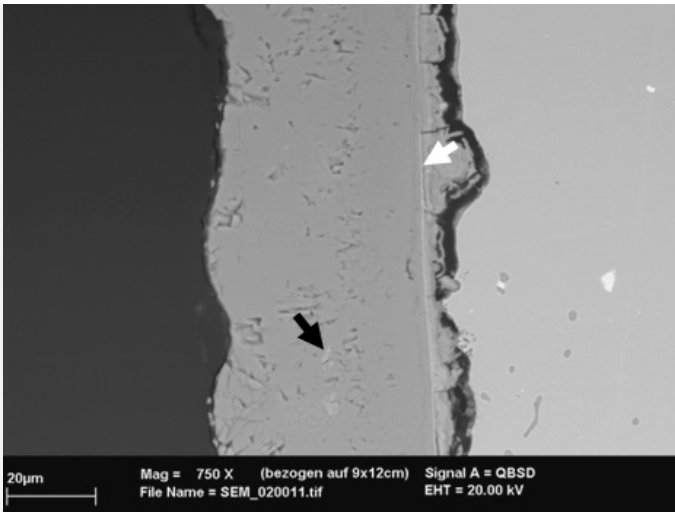
Table 2: Chemical composition (mass %) of the corrosion layers from Fig. 15. Method of analysis: SEM/EDS, Laboratory of Analytical Chemistry, Empa.



Credit HE-Arc CR.

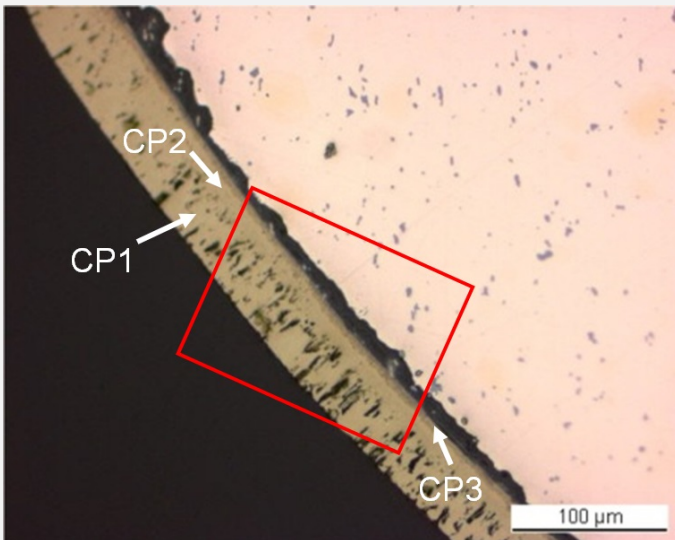
Fig. 13: SEM image of the metal sample from Fig. 9 (detail), SE-mode. The crack between the remaining metal and the corrosion layers is clearly visible,

Fig. 14: SEM image similar to Fig. 13, BSE-mode. A thin line is visible (white arrow) differentiating the inner Sn-rich layer from the intermediate and outer chalcopyrite layers. The latter contains bright covellite inclusions (black arrow) and pores,



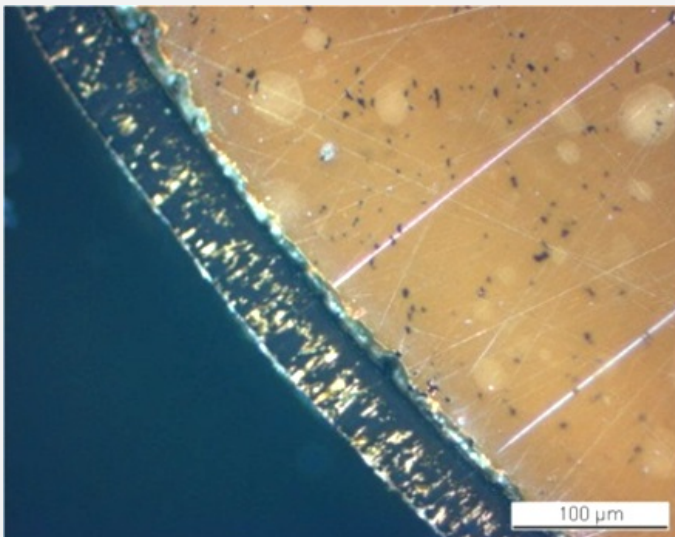
Credit HE-Arc CR.

Fig. 15: Micrograph of the metal sample from Fig. 9 (detail) and corresponding to the stratigraphy of Fig. 20, unetched, bright field. The area selected for elemental chemical distribution (Fig. 17) is marked by a red rectangle,



Credit HE-Arc CR.

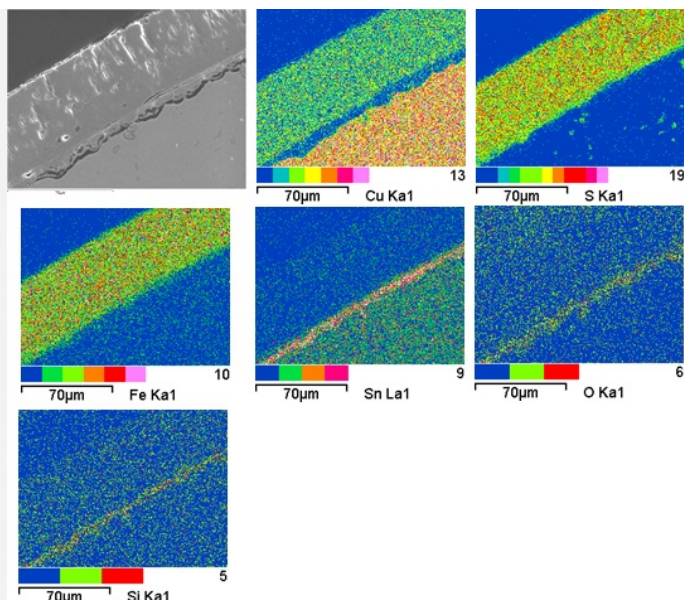
Fig. 16: Micrograph similar to Fig. 15, polarised light,



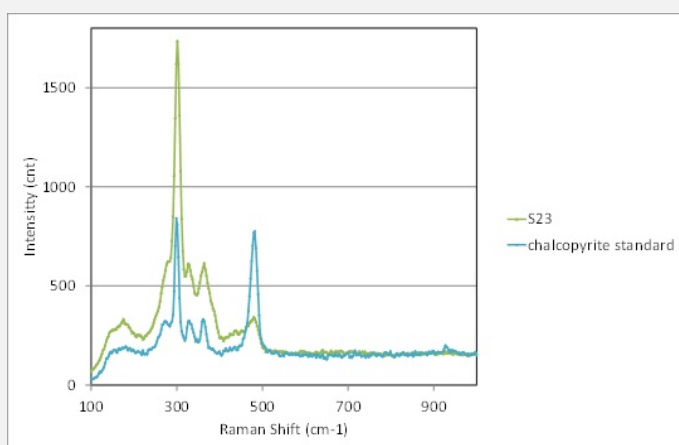
Credit HE-Arc CR.

Fig. 17: SEM image and elemental chemical distribution of a selected area of Fig. 15 (rotated by 90°). Method of examination: SEM/EDS, Laboratory of Analytical Chemistry, Empa,

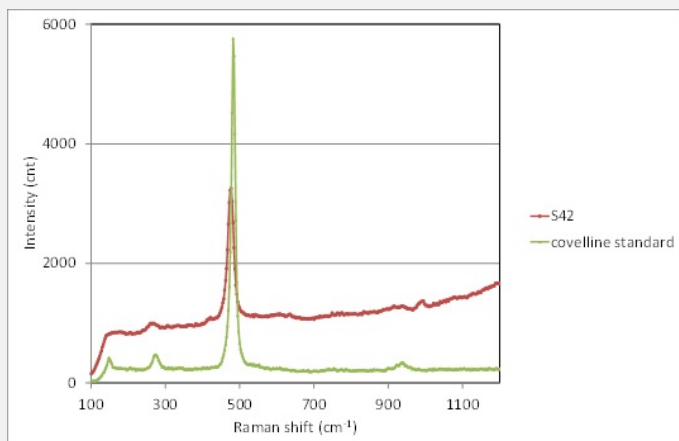




Credit Empa.



Credit SNM.



Credit SNM.

Fig. 18: Raman spectrum of the outermost layer (S23) of Fig.14 compared to a chalcopyrite standard spectrum. Settings: laser wavelength 532nm, acquisition time 50s, 4 accumulations, filter D2 (0.75-0.8mW), hole 1000, slit 100, grating 600. Method of analysis: Raman spectroscopy, Lab of Swiss National Museum, Affoltern a. Albis ZH,

Fig. 19: Raman spectrum of the inclusions of the outermost layer (S42) of Fig. 14 compared to a covelline / covellite standard spectrum. Settings: laser wavelength 532nm, acquisition time 10s, 5 accumulations, D2 (0.75-0.8mW), hole 500, slit 80, grating 600. Method of analysis: Raman spectroscopy, Lab of Swiss National Museum, Affoltern a. Albis ZH,6

Corrosion form	Uniform - pitting
Corrosion type	Type I (Robbiola)

#### Complementary information

Schweizer (1994) indicates that CP3 shows evidence of pseudomorphic replacement of metal grains by corrosion products that we did not observe.

## ✧ MiCorr stratigraphy(ies) – CS

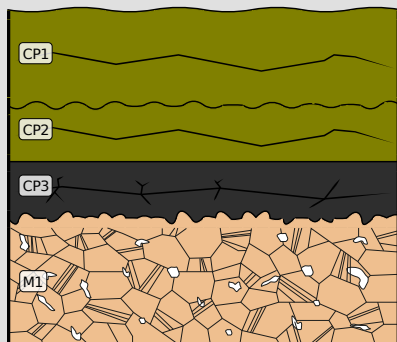


Fig. 20: Stratigraphic representation of the sample taken from the pin without head in cross-section (dark field) using the MiCorr application. The characteristics of the strata are only accessible by clicking on the drawing that redirects you to the search tool by stratigraphy representation. This representation can be compared to Fig. 15, Credit HE-Arc CR.

## ✧ Synthesis of the binocular / cross-section examination of the corrosion structure

The stratigraphies observed under binocular and cross-section are rather similar. It is not possible though to distinguish the compact underlayer (CP2 in cross-section) under binocular.

## ✧ Conclusion

The pin is made from tin bronze and has been annealed after cold working. It is covered with a regular, dense brown-yellow patina typical of lake context (Schweizer 1994). The inner, thin Sn-rich corrosion layer contains soil elements such as Si. The brown-yellow, thick intermediate and outer corrosion layers have the composition of chalcopryrite. This object was certainly abandoned rather quickly in an anaerobic, humid and S and Fe-rich environment, favouring the formation of the above mentioned compound. The limit of the original surface can be located between the chalcopryrite and the Cu depleted but Sn-rich inner corrosion layer. Thus, the corrosion is a type 1 according to Robbiola et al. 1998.

## ✧ References

### References on object and sample

#### *References object*

1. Rychner-Faraggi A-M. (1993) Hauterive – Champréveyres 9. Métal et parure au Bronze final. Archéologie neuchâteloise, 17 (Neuchâtel).
2. Hochuli, S. et al. (1988) SPM III Bronzezeit, Verlag Schweizerische Gesellschaft für Ur- und Frühgeschichte Basel, 76-77, 379.

#### *References sample*

3. Empa Report 137 695/1991, P.O. Boll.
4. Rapport d'examen, Lab. Musées d'Art et d'Histoire, Geneva GE, 87-194 à 87-197.
5. Schweizer, F. (1994) Bronze objects from Lake sites: from patina to bibliography. In: Ancient and historic metals, conservation and scientific research (eds. Scott, D.A., Podany, J. and Considine B.B.), The Getty Conservation Institute, 33-50.

### References on analytic methods and interpretation

6. Robbiola, L., Blengino, J-M., Fiaud, C. (1998) Morphology and mechanisms of formation of natural patinas on archaeological Cu-Sn alloys, Corrosion Science, 40, 12, 2083-2111.

